Research Square

Preprints are preliminary reports that have not undergone peer review.
They should not be considered conclusive, used to inform clinical practice,
or referenced by the media as validated information.

A MBene-based electrochemical aptasensor for label-free detection of EpCAM-overexpressing cancer cells

Min Li
the First Affiliated Hospital of Xi'an Jiaotong University
Yue Jiang
The Hong Kong University of Science and Technology (Guangzhou)
Yang Huang
The Hong Kong University of Science and Technology (Guangzhou)
Wei Chen
Xi'an Jiaotong University
Yan Li
Xi'an Jiaotong University
Dongxin Liang
the First Affiliated Hospital of Xi'an Jiaotong University
Yuqi Wang
the First Affiliated Hospital of Xi'an Jiaotong University
Qian Qie
the First Affiliated Hospital of Xi'an Jiaotong University
Jiaxian Yuan
Xi'an Jiaotong University
Jiahui Zhang
the First Affiliated Hospital of Xi'an Jiaotong University
Yuan Zhang
the First Affiliated Hospital of Xi'an Jiaotong University
Siyu Yang
the First Affiliated Hospital of Xi'an Jiaotong University
Xin He
the First Affiliated Hospital of Xi'an Jiaotong University
Zhaoyi Zhang
the First Affiliated Hospital of Xi'an Jiaotong University
Liping Du
Xi'an Jiaotong University

Chunsheng Wu

wuchunsheng@xjtu.edu.cn

Xi'an Jiaotong University

Qiling Li

the First Affiliated Hospital of Xi’an Jiaotong University

Article

Keywords: MBene, electrochemical aptasensor, EpCAM, cancer cell detection

Posted Date: July 8th, 2026

DOI: https://doi.org/10.21203/rs.3.rs-9835867/v1

License: This work is licensed under a Creative Commons Attribution 4.0 International License.
Read Full License

Additional Declarations: No competing interests reported.

Abstract

Epithelial cell adhesion molecule (EpCAM) is widely overexpressed in epithelial-derived malignancies, serving as an important biomarker for cancer cell detection. Conventional EpCAM detection strategies rely on labeling and multi-step processing, which may limit their point-of-care applications. Herein, a label-free electrochemical aptasensor based on MBene is presented for the detection of EpCAM-overexpressing cancer cells. MBene nanosheets provide a conductive and functional sensing interface that facilitates electron transfer and stable immobilization of EpCAM-specific aptamers. The aptasensor exhibits a linear response to EpCAM protein over a range of 10 fg mL^{-1} to 100 pg mL^{-1}, with a detection limit of 8.86 fg mL^{-1}. For EpCAM-overexpressing cancer cells, a concentration-dependent response is observed from 10^1 to 10^5 cells mL^{-1}, achieving a detection limit of 7 cells mL^{-1}. The platform also demonstrates good specificity, reproducibility, and storage stability. Performance in complex biological matrices is further evaluated using 44 clinical endometrial cytological samples, where the electrochemical response enables effective discrimination between malignant and benign cases, yielding an area under the receiver operating characteristic curve of 0.897. This work highlights the potential of MBene-based electrochemical aptasensing as a label-free and accessible strategy for detecting EpCAM-overexpressing cancer cells, with possible applications in clinical analysis and point-of-care diagnostics.

Introduction

Accurate and sensitive detection of tumor cells remains a central challenge in cancer diagnostics and early intervention. Among various molecular biomarkers, epithelial cell adhesion molecule (EpCAM) is a transmembrane glycoprotein that is extensively overexpressed in a wide spectrum of epithelial-derived malignancies, including breast, colorectal, lung, and gynecologic cancers [1–3]. EpCAM plays a critical role in tumor cell proliferation, migration, and signaling, thereby serving as an important biomarker for malignant cell identification [2–4].Despite its clinical importance, EpCAM detection in routine practice still relies predominantly on immunohistochemistry, enzyme-linked immunosorbent assay, and flow cytometry. These approaches involve labor-intensive labeling procedures, multiple processing steps, and are highly dependent on specialized equipment and expertise, which limits their applicability in point-of-care settings [5–7]. Therefore, developing alternative analytical strategies that balance operational simplicity with reliable analytical performance remains of considerable interest for clinical cancer diagnostics.

Electrochemical biosensors offer a promising approach, with advantages including high sensitivity, rapid response, operational simplicity, low cost, and compatible with portable devices [8,9]. Among them, electrochemical impedance spectroscopy (EIS) enables label-free monitoring of interfacial changes [10], allowing sensitive detection of biomolecular and cellular interactions [11,12]. In addition, screen-printed gold electrodes (SPGEs) provide a disposable, scalable, and reproducible platform suitable for practical applications [13–16]. Moreover, the all-in-one integrated three-electrode configuration of SPGEs enables

miniaturized and user-friendly measurements, which is advantageous for point-of-care applications. Despite these benefits, many reported electrochemical sensing systems rely on complex surface modification strategies or intricate signal amplification mechanisms, which may compromise their practicality and reproducibility in translational applications.

Selective molecular recognition is essential for cancer cell detection. Compared with antibodies [17], aptamers possess advantages such as synthetic accessibility, high affinity and specificity, lower production costs, chemical and thermal stability, and facile functional modification [18–20]. Therefore, EpCAM-specific aptamers provide a reliable molecular recognition strategy for the selective capture of EpCAM- overexpressing cancer cells on electrochemical sensing interfaces [21]. However, constructing a high-performance sensing interface necessitates both efficient electron transfer and stable aptamer immobilization.

Two-dimensional nanomaterials, such as graphene and MXene, have been widely investigated for electrochemical biosensing owing to their high surface areas and electrical conductivity [22–24]. As a boride-based analogue within the MXene-related family, MBene shares several advantageous characteristics, including favorable electrical conductivity, large active surface areas, and abundant surface-active sites [24,25]. These properties enable MBene to facilitate interfacial electron transfer and support biomolecular immobilization [26]. In this context, MBene can serve as an ideal functional matrix to achieve cell-level detection through a straightforward and label-free sensing architecture, aligning with the requirements of accessible diagnostic tools.

In this study, an integrated MBene-based electrochemical aptasensing platform was developed for label-free detection of EpCAM-overexpressing cancer cells (Fig. 1). Two-dimensional MBene nanosheets were assembled onto the working electrode of SPGEs to construct a conductive and biocompatible sensing interface, followed by immobilization of EpCAM-specific aptamers for selective molecular recognition. The analytical performance of the platform was systematically evaluated using EpCAM protein standards and cancer cell lines. Furthermore, moving beyond conventional spiked or simulated laboratory validation, clinical endometrial cytological samples were analyzed to examine the platform's performance in complex biological matrices, providing preliminary evidence for its potential applicability in real-world settings.

Results and discussion

Characterization of MBene

The synthesis and structural transformation of the Cr_2AlB_2 precursor into two-dimensional CrB MBene nanosheets were systematically characterized to evaluate their suitability as an electrochemical sensing interface. SEM results revealed a pronounced morphological evolution. The precursor Cr_2AlB_2 exhibited compact, block-like particles with smooth surfaces (Fig. 2a), consistent with its typical three-

dimensional MAB crystal structure [27]. After selective etching, the resulting CrB MBene displayed a markedly rougher and porous morphology with an open, layered architecture (Fig. 2b), which was characteristic of two-dimensional MBene materials [27,28]. This morphological transformation was attributed to the selective removal of Al layers, which weakened the interlayer bonding and facilitated exfoliation into two-dimensional nanosheets.

The phase transition was further confirmed by XRD analysis (Fig. 2c). The diffraction peaks of the Cr_2AlB_2 precursor matched well with the standard JCPDS card (No. 72-1847) [29]. After HCl etching, the characteristic peaks of Cr_2AlB_2 significantly decreased or disappeared, accompanied by the emergence of broader peaks corresponding to the CrB phase (JCPDS No. 75-1159), which was in good agreement with previous researches [27,30]. A broader peak width and a lower diffraction intensity indicated a decrease in crystallinity, confirming the successful formation of two-dimensional MBene nanosheets.

The surface composition and chemical states of MBene were examined by XPS. The survey spectrum confirmed the presence of Cr, B, C, and O elements(Fig. 2d). Critically, only a weak Al 2p signal at approximately 74.7 eV was detected (Fig. 2e), indicating the nearly complete removal of Al layer from the MAB precursor [27].The B 1s spectrum exhibited a dominant peak at approximately 187.9 eV, corresponding to Cr–B bonding (Fig. 2e), accompanied by minor contributions assigned to surface oxidation (B_2O_{3-x} at 190.38 eV and B_2O_3 at 192.06 eV) [31]. Similarly, the Cr 2p spectrum showed characteristic Cr–B bonding at approximately 574.57 eV (Cr $2p_{3/2}$) and 583.59 eV (Cr $2p_{1/2}$) (Fig. 2e), along with weak Cr–O signals at higher binding energies (577.11 eV and 587.31 eV) [32].

FTIR spectroscopy provided the complementary evidence of surface termination groups (Fig. 2f). An absorption band around 3400 cm^{-1} was assigned to the stretching and bending vibrations of surface –OH groups, indicating hydroxyl terminations on the MBene surface [33]. Peaks in the range of 1050–1150 cm^{-1} were attributed to B–O vibrations, suggesting slight surface oxidation during the etching or drying process [33–35]. Additionally, characteristic absorption bands between 600 and 800 cm^{-1} were assigned to Cr–B vibrations, confirming the preservation of the boride framework after Al removal.

Collectively, these findings verified the successful synthesis of two-dimensional CrB MBenes with a layered morphology, high surface roughness, and oxygen-containing surface terminations. These structural and chemical features provided a conductive, chemically active interface, which was suitable for efficient electron transfer and stable aptamer immobilization in electrochemical cancer cell detection.

Verification of stepwise biosensing interface assembly

The stepwise fabrication of the MCH/Aptamer/MBene/SPGE platform was illustrated in Scheme 1 and systematically verified by electrochemical characterization, surface morphological analysis, and fluorescence measurements.

CV and EIS were conducted to monitor the interfacial electron-transfer behavior at each modification stage **(**Fig. 3a-b**)**. To quantify these interfacial changes, the EIS data were fitted using a classical Randles equivalent circuit model **(inset of** Fig. 3b**)**. This model comprised the solution resistance (R_s), double-layer capacitance (C), charge transfer resistance (R_{ct}), and Warburg impedance (Z_w). Among these parameters, R_{ct} served as a sensitive indicator for monitoring surface modifications. The bare SPGE exhibited well-defined redox peaks and a low R_{ct}, indicating good electron transport at the electrode surface. Upon modification with MBene nanosheet, the redox peak current increased in the CV curve while R_{ct} decreased in the Nyquist plot of EIS, indicating that the modification of MBene enhanced electron transfer kinetics at the interface due to the high conductivity and large surface area [36,37]. In contrast, subsequent immobilization of the EpCAM aptamer and MCH blocking led to a gradual decrease in peak current and a corresponding increase in R_{ct} **(**Fig. 3a-b**)**, which can be attributed to the formation of insulating biomolecular layers that partially impeded interfacial electron exchange. Notably, incubation with the EpCAM protein produced a further increase in R_{ct}, confirming successful bio-recognition and target capture at the sensing interface **(**Fig. 3b-c**)**.

AFM provided complementary morphological evidence of the progressive interface construction **(**Fig. 3d**)**. Quantitative roughness analysis revealed a stepwise increase in both average roughness (R_a) and root mean square roughness (R_q) throughout the assembly process. The bare SPGE exhibited a relatively smooth surface (R_a/R_q: 66.72/90.03 nm) **(**Fig. 3d-i**)**, whereas MBene modification produced a markedly roughen and layered topology (R_a/R_q: 101.57/145.75 nm) **(Supplementary Fig. 1a)**. Following aptamer immobilization, the surface roughness further increased (R_a/R_q: 135.19/172.12 nm) **(Supplementary Fig. 1b)**, indicating successful anchoring of the aptamers. After EpCAM protein binding, the highest roughness values were observed (R_a/R_q: 161.56/195.14 nm) **(**Fig. 3d-i**i)**, consistent with target accumulation on the sensing interface [38,39].

Fluorescence measurements using a FAM-labeled EpCAM aptamer was employed as an auxiliary method to verify the interfacial assembly and target recognition process. Mbene/SPGE showed no fluorescence signal **(Supplementary Fig. 2a)**. Upon the immobilization of FAM-labeled EpCAM aptamers, a strong fluorescence signal was observed on the electrode surface **(Supplementary Fig. 2b)**, confirming successful aptamer loading onto the sensing interface. Following incubation with the EpCAM protein solution, a noticeable decrease in fluorescence intensity was recorded **(Supplementary Fig. 2c)**. This phenomenon may be associated with several factors, including conformational rearrangement of the aptamer upon target binding, steric hindrance effects, or changes in local microenvironment of fluorophore at the interface, although the exact mechanism requires further investigation [40–42]. Collectively, these observation, together with the electrochemical data, supported the interactions between aptamer and EpCAM target.

Optimization of experimental parameters

To achieve optimal sensing performance, key experimental parameters were systematically optimized. The electrochemical response was quantified by the relative change in charge transfer resistance ($\triangle R_{ct}$), defined as the difference between R_{ct} measured after target binding and that obtained after MCH blocking.

The concentration of MBene was optimized in a range of 0–1 mg mL^{-1} **(Supplementary Fig. 3a)**. The $\triangle R_{ct}$ increased with MBene concentration, reflecting improved electron transfer efficiency and increased electroactive surface area for aptamer immobilization. A maximum response was observed at 100 µg mL^{-1}. Therefore, 100 µg mL^{-1} was selected as the optimal MBene concentration, providing a balanced interface that combined high conductivity with sufficient surface area for aptamer immobilization.

The effect of aptamer concentration on sensor response was subsequently investigated **(Supplementary Fig. 3b)**. The $\triangle R_{ct}$ increased steadily as the aptamer concentration rose from 0.2 to 1 µM and then plateaued, indicating saturation of available binding sites. Accordingly, 1 µM was chosen as the concentration of aptamers for subsequent experiments.

In addition, the incubation time was optimized to ensure efficient target recognition **(Supplementary Fig. 3c)**. The $\triangle R_{ct}$ increased progressively with incubation time and reached a steady maximum at 60 min, indicating that binding equilibrium was achieved. Based on these results, the optimized conditions were applied in all subsequent analytical performance evaluations.

Validation of EpCAM expression on cell lines

To establish reliable cellular models for evaluating EpCAM-targeted electrochemical sensing, the expression level of EpCAM was examined in Ishikawa and HEK293T cell lines at both the transcriptional and protein levels. As shown in Fig. 3e, RT-qPCR analysis revealed a markedly higher EpCAM mRNA expression in Ishikawa cells compared with HEK293T cells ($p < 0.0001$). Consistently, WB analysis showed a strong EpCAM protein band in Ishikawa cells, whereas EpCAM expression in HEK293T cells was negligible **(**Fig. 3f and **Supplementary Fig. 4)**. Quantitative analysis confirmed a highly significant difference between the two cell lines ($p < 0.0001$) **(**Fig. 3f**)**. Therefore, Ishikawa cells were employed as an EpCAM-overexpressing cancer cell model, while HEK293T cells served as an EpCAM-negative control for all subsequent aptasensor experiments.

Electrochemical analytical performance

The electrochemical analytical performance of the optimized MCH/Aptamer/MBene/ SPGE biosensor was evaluated via EIS by monitoring $\triangle R_{ct}$ in response to EpCAM protein and EpCAM-overexpressing cancer cells, independently.

For the detection of EpCAM protein, $\triangle R_{ct}$ increased proportionally with protein concentration (Fig. 4a). A linear relationship was obtained over the concentration range from 10 fg mL^{-1} to 100 pg mL^{-1}, as described by the regression equation: $\triangle R_{ct}$ = 1127.47 + 329.46 Lg C_{EpCAM} (R^2 = 0.99) (Fig. 4d). Based on the 3σ criterion (S / N = 3), the limit of detection (LOD) was calculated to be 8.86 fg mL^{-1}, indicating a high sensitivity for low-abundance EpCAM protein.

The applicability of the biosensor for cell-level detection was further investigated using EpCAM-overexpressing Ishikawa cells. As shown in Fig. 4b, the $\triangle R_{ct}$ increased consistently with growing cell concentration, exhibiting a linear response in the range of 10^1 to10^5 cells mL^{-1}. The corresponding linear equation was: $\triangle R_{ct}$ = 515.77 + 381.12 Lg $C_{Ishikawa}$ (R^2 = 0.99) (Fig. 4e), with a calculated LOD of 7 cells mL^{-1}.

These results indicate that the proposed aptasensor enabled sensitive detection of EpCAM at both molecular and cellular levels. To benchmark its analytical performance, the proposed MBene-based biosensor was compared with previously reported EpCAM detection platforms **(Supplementary Table 1)** [43–53]. The LODs achieved in this study were comparable to or lower than those reported for many existing systems. This performance can be attributed to the synergistic contribution of MBene based electron transfer and aptamer-mediated high-affinity molecular recognition.

Specificity, reproducibility, and stability

The specificity of the MCH/Aptamer/MBene/SPGE biosensor was evaluated using EpCAM-negative HEK293T cells as control to assess potential nonspecific interactions from cell-surface biomolecules. As shown in Fig. 4g, the electrochemical impedance response ($\triangle R_{ct}$) generated by EpCAM-overexpressing Ishikawa cells (10^5 cells mL^{-1}) was markedly higher than that obtained for HEK293T cells at the same concentration ($p < 0.0001$). To visually confirm this selective capture capability, fluorescence imaging based on DAPI staining was performed. A high density of Ishikawa cells was clearly observed on the electrode surface, whereas negligible cell adhesion was detected for the HEK293T cells, even at a tenfold higher concentration **(Supplementary Fig. 5)**. To further assess anti-interference performance, HEK293T cells (10^5 cells mL^{-1}) were introduced as background interference and mixed with gradient concentrations of Ishikawa cells (Fig. 4c). Under these conditions, the resulting calibration curve ($\triangle R_{ct}$ = 684.02 + 298.65 Lg $C_{Mixture}$, R^2 = 0.99, Fig. 4f) remained similar with that of Ishikawa cells alone (Fig. 4e), indicating that nonspecific cells exerted minimal influence on the sensing response. The specificity originates from the strong and specific interaction between the EpCAM aptamer and its membrane protein target.

The reproducibility was evaluated by three independently fabricated electrodes across varying Ishikawa cell concentrations (10^1, 10^3, and 10^5 cells mL^{-1}). As shown in Fig. 4h, the relative standard deviations for all tested concentrations were below 5%, demonstrating reliable fabrication consistency and measurement reliability.

The storage stability of the aptasensor was examined by storing the electrodes at 4℃ and periodically recording their electrochemical response. The biosensor retained 98.31% of its initial signal after 3 days, and maintained 97.47%, 96.60%, 95.29%, and 92.28% of the original response after 5, 7, 9, and 14 days, respectively (Fig. 4i). These results indicate satisfactory long-term stability of the MCH/Aptamer/MBene/ SPGE platform, making it suitable for practical point-of-care applications.

Real clinical sample analysis

The clinical relevance of EpCAM as a cancer-associated biomarker was first confirmed by immunohistochemical staining of 22 paired human endometrial tissue specimens (Fig. 5a-b). Quantitative analysis revealed significantly higher EpCAM expression in endometrial cancer tissues (IOD: 7583.79 ± 1325.47) compared with adjacent non-cancerous controls (IOD: 2709.38 ± 489.49) ($p < 0.0001$) (Fig. 5c). These findings verified the differential expression of EpCAM between malignant and non-malignant tissues, thereby providing pathological evidence to support EpCAM as a valid molecular target for EpCAM-overexpressing cancer cell detection.

The applicability of the proposed MBene-based electrochemical aptasensor was further evaluated using real clinical cytological specimens in complex biological matrices. The collection and preparation procedure of endometrial cytological samples using Li-Brush was schematically illustrated in Fig. 5d. Subsequently, 44 clinically confirmed endometrial cytological samples were analyzed, including 22 endometrial cancer cases and 22 benign controls (Fig. 5e). Detailed clinical characteristics of the study cohort were summarized in **Supplementary Table 2**. As shown in Fig. 5f, malignant endometrial cytological samples generated significantly higher impedance responses ($\triangle R_{ct}$) than benign controls ($p < 0.0001$), which was consistent with elevated EpCAM expression observed at the tissue level.

To maximize the diagnostic utility of the electrochemical signals, four supervised machine learning models were implemented and compared. Among the evaluated algorithms, the logistic regression model demonstrated the most balanced performance, achieving a sensitivity of 86.36%, a specificity of 86.36%, and an overall accuracy of 86.36%, with an AUC of 0.897 (Fig. 5g and **Supplementary Table 3)**. The corresponding classification threshold ($\triangle R_{ct}$ = 720 Ω) enabled direct discrimination between benign and malignant samples, thereby facilitating straightforward interpretation of electrochemical response signals in practical applications.

Compared with conventional clinical diagnostic modalities, the developed aptasensor demonstrated competitive and relatively balanced diagnostic performance. Transvaginal ultrasound typically showed sensitivities of 70.9% − 81.4% and specificities of 80.6% − 92.0% [54], whereas serum biomarkers such as carbohydrate antigen 125 and human epididymis protein 4 generally exhibited lower sensitivities ranging from 25.0% − 46.0% and 56.0% − 82.0%, and specificities of 71.0% − 91.0% and 80.0% − 92.0%, respectively [55]. Endometrial biopsy demonstrated a sensitivity of 73.5% and a specificity of 99.4% but required invasive tissue sampling [56]. In contrast, the proposed electrochemical platform achieved

balanced diagnostic performance (sensitivity: 86.36%, specificity: 86.36%, AUC:0.897) through a label-free and cytology-based detection strategy. Furthermore, this electrochemical approach relied on a relatively simple operational workflow and reduced dependence on subjective pathological interpretation.

Nevertheless, several limitations should be acknowledged. The present study was limited by the relatively small cohort size, and additional validation using larger, multi-center clinical populations will be required in future studies. Moreover, further optimization of the sensing interface architectures and data analysis strategy may improve clinical sensitivity and robustness. Despite these limitations, the use of patient-derived clinical samples rather than simulated or artificially spiked systems provided translational evidence supporting the feasibility of the proposed sensing strategy.

In conclusion, this study developed an MBene-based electrochemical aptasensor for label-free detection of EpCAM-overexpressing cancer cells. The platform achieved sensitive detection with satisfactory specificity, reproducibility, and storage stability, benefiting from the conductive and functional properties of MBene nanosheets. Preliminary validation using patient-derived clinical endometrial cytological samples demonstrated that the electrochemical response could effectively discriminate between malignant and benign cases. These results supported the applicability of this EpCAM-targeted electrochemical sensing strategy for cell-level analysis in complex biological samples. Overall, this work established a feasible electrochemical sensing approach for label-free detection of EpCAM-overexpressing cancer cells and expanded the application of MBene nanomaterials in biosensing and clinical analysis. The proposed platform provided a complementary strategy for potential use in clinical and point-of-care settings.

Methods

Reagents and materials

All chemicals and reagents were of analytical grade and used as received without further purification. Cr_2AlB_2 (99% purity) powder was purchased from Foshan Xinxi Technology (Guangdong, China). Hydrochloric acid (HCl, 36.0%~38.0% purity) was obtained from Guangshi Regent Technology Co., Ltd (Guangdong, China). Tris (2-carboxyethyl) phosphine, 6-mercapto-1-hexanol (MCH), and Tris-HCl buffer were obtained from Aladdin Biochemical Technology Co., Ltd. (Shanghai, China). Potassium ferricyanide ($Fe(CN)_6^{3-}$) and potassium ferrocyanide ($Fe(CN)_6^{4-}$) were supplied by Sinopharm Chemical Reagent Co., Ltd. (Shanghai, China). SPGEs were acquired from Weihai Poten Technology (Weihai, China). The thiolated EpCAM aptamer and fluorescein amidite (FAM)-labeled EpCAM aptamer were synthesized and purchased from Sangon Biotech Co., Ltd. (Shanghai, China). The sequence was listed as follows: 5’-SH-$(CH_2)_6$-TTTTTTCACTACAGAGGTTGCGTCTGTCCCAC GTTGTCATGGGGGGTTGGCCTG-3’. The FAM-labeled EpCAM aptamer was obtained by conjugating FAM to the 3’ terminus. HEK293T cells were obtained from the Cell Bank of the Chinese Academy of Sciences (Shanghai, China), and Ishikawa cells were purchased from Procell Life Science & Technology Co., Ltd. (Wuhan, China). Dulbecco’s modified

Eagle's medium, fetal bovine serum, penicillin- streptomycin, trypsin-EDTA (0.25%), phosphate-buffered saline (PBS, 10 mM, pH 7.4), and 4',6-diamidino-2-phenylindole (DAPI) were purchased from Gibco (USA). The high-efficiency RNA extraction reagent was obtained from Kermey Biotech Co., Ltd. (Henan, China). Reverse transcription and qPCR reagents, including the TolaScript All-in-One RT Easy Mix (with 2-step gDNA Erase-Out) and Universal SYBR Green qPCR Master Mix, were purchased from Tolo Biotech Co., Ltd. (Shanghai, China). Primers were synthesized by Tsingke Biotechnology Co., Ltd. (Beijing, China). For western blotting, RIPA lysis buffer was purchased from Beyotime Biotechnology (Shanghai, China). Rabbit anti-human EpCAM and mouse anti-human α-Tubulin antibodies were obtained from UpingBio Co., Ltd. (Zhejiang, China), while horseradish peroxidase-conjugated goat anti-rabbit and goat anti-mouse secondary antibodies were purchased from Kermey Co., Ltd. (Henan, China). Electrophoresis was performed using Bio-Rad equipment with 10% sodium dodecyl sulfate-polyacrylamide gels, and chemiluminescent substrates were obtained from Kejie Co., Ltd. (Shanghai, China). Clinical endometrial samples were collected from the First Affiliated Hospital of Xi'an Jiaotong University under approved ethical protocols.

Synthesis and characterization of MBene

Two-dimensional CrB MBene nanosheets were synthesized via a selective etching strategy following previously reported methods with minor modifications [29,30]. Briefly, 1 g of Cr_2AlB_2 precursor powder was immersed in 30 mL of 2 M HCl and magnetically stirred at room temperature for 96 h to selectively remove the interleaved aluminum layers. After etching, the resulting suspension was centrifuged at 8000 rpm for 5 min, and the solid residue was repeatedly washed with deionized water until the supernatant reached a neutral pH. The purified MBene was subsequently freeze-dried for 48 hours to obtain a stable powder for subsequent use.

Structural and morphological investigations were conducted systematically. Surface morphology was examined using SEM (MIRA4, Czech Republic) and AFM (SPM-9700HT, Japan). Crystal structure and phase purity were confirmed via XRD (Aeris, UK). Surface elemental composition and chemical valence states were determined via XPS (K-Alpha, USA). Surface functional groups were analyzed using FTIR (Vertex 70V, Germany) .

Aptasensor fabrication and electrochemical measurement

The electrochemical aptasensor was fabricated via stepwise assembly on integrated SPGEs. These SPGE chips featured an all-in-one three-electrode configuration, comprising a gold working electrode, a bare gold counter electrode, and an Ag/AgCl reference electrode on a single substrate. Prior to modification, the SPGEs electrodes were sequentially rinsed with 75% ethanol and ultrapure water until stable cyclic voltammetry (CV) responses were obtained. MBene nanosheets were dispersed ultrasonically and drop-cast onto the working electrode surface of SPGEs, followed by drying at 37 ℃ to form a conductive interface. For biorecognition, thiolated EpCAM aptamers were reduced with 1mM Tris (2-carboxyethyl) phosphine for 1 h and immobilized onto the MBene-modified electrode by overnight incubation at 4 ℃. After rinsing, non-specific sites were blocked with 10 μM MCH for 1 h to obtain the

final MCH/Aptamer/MBene/SPGE biosensor. Well-prepared electrodes were dried with N_2 blow and stored at 4℃ prior to use.

Electrochemical measurements were performed on an electrochemical workstation (Zahner ZenniumE, Germany) within a Faraday cage to minimize environmental interference. All measurements were conducted in 10 mM PBS containing 1 mM $[Fe(CN)_6]^{3-/4-}$. CV was recorded from − 0.2 V to + 0.9 V at a scan rate of 100 mV s^{-1}. EIS was measured over a frequency range of 0.1 Hz to 10^5 Hz with an AC amplitude of 5 mV at the open-circuit potential.

Cell culture and EpCAM expression analysis

Ishikawa and HEK293T cell lines were cultured in Dulbecco's modified Eagle's medium supplemented with 10% fetal bovine serum and 1% penicillin-streptomycin at 37℃ under 5% CO_2 atmosphere. Cells were harvested at approximately 90% confluence and resuspended in PBS at desired concentrations for subsequent experiments.

EpCAM expression levels were assessed by real-time quantitative reverse transcription polymerase chain reaction (RT-qPCR) and Western blot (WB) analysis. Total RNA was extracted and reverse-transcribed into cDNA according to manufacturer protocols. RT-qPCR was performed using Universal SYBR Green qPCR Master Mix on a real-time PCR system (Bioer QG-9600, China), with primer sequences listed in **Supplementary Table 4**. Relative mRNA levels was calculated using the $2^{-\Delta\Delta Ct}$ method, with α-Tublin serving as the internal reference.

For WB analysis, cells were lysed in RIPA buffer, and total protein concentrations were quantified prior to separation by sodium dodecyl sulfate-polyacrylamide gel electrophoresis. Proteins were transferred onto polyvinylidene fluoride membranes and sequentially incubated with primary antibodies (anti-EpCAM and α-Tubulin), followed by appropriate horseradish peroxidase-conjugated secondary antibodies. Protein bands were visualized using a chemiluminescence imaging systems and quantified with ImageJ software.

Analytical performance for protein and cell detection

The analytical performance of MCH/Aptamer/MBene/SPGE biosensor was comprehensively evaluated using EpCAM protein standards and cell suspensions. Experimental parameters, including MBene concentration, aptamer loading, and target incubation time, were optimized to maximize the electrochemical response.

Sensitivity was assessed by recording EIS responses to EpCAM-positive Ishikawa cell suspensions over a concentration range of 10^1-10^5 cells mL^{-1} at 37℃. Specificity was evaluated using EpCAM-negative HEK293T cells (10^5 cells mL^{-1}) as control and as background interference mixed with gradient concentrations of Ishikawa cells. PBS served as the blank control. Captured cells on the electrode surface were visually confirmed by DAPI staining and fluorescence microscopy. Reproducibility was assessed using three independently fabricated biosensors under identical conditions. In order to test the

long-term stability, the well-prepared MCH/Aptamer/MBene/ SPGE biosensor was blow-dried with N_2 and stored at 4℃ for different time intervals. The EIS response was evaluated by monitoring Ishikawa cells of 10^4 cells mL^{-1} with stored biosensors.

Clinical sample validation

The clinical relevance of EpCAM was first evaluated by immunohistochemical staining of paired endometrial cancer and adjacent non-cancerous tissues. EpCAM expression levels were quantified by the integrated optical density (IOD) analysis. Subsequently, the performance of MCH/Aptamer/MBene/SPGE biosensors was assessed using real clinical endometrial cytological samples collected from patients undergoing surgery between August and December 2025. Cytological samples were collected by Li-Brush [57], followed by centrifugation and resuspension in PBS, and were directly subjected to EIS measurements following the same protocol as applied for cell lines assay. Clinical samples were classified as malignant or benign groups according to postoperative histopathological diagnosis.

This study was conducted in strict accordance with the Declaration of Helsinki and approved by the Institutional Ethics Committee of the First Affiliated Hospital of Xi'an Jiaotong University (Approval No: XJTUIAF2025LSYY- 813), with informed consent obtained from all participants.

Statistical Analysis

All experiments were performed in at least three independent repeats, and data were presented as mean ± standard deviation. Statistical analyses were conducted using GraphPad Prism 10.0. Differences between groups were analyzed using Student's *t*-test or one-way analysis of variance, with a two-tailed $p < 0.05$ considered statistically significant.

To further assess the diagnostic performance of the electrochemical aptasensor in clinical cytological specimens, machine learning-based classification was performed using Python. With postoperative histopathology as the reference standard, electrochemical response data from clinical endometrial cytological samples were analyzed using a leave-one-out cross-validation strategy to ensure reliable performance estimation with the limited sample size. Several supervised learning models, including k-nearest neighbors, decision tree, support vector machine with radial basis function kernel, and logistic regression, were evaluated. Diagnostic performance was assessed in terms of sensitivity, specificity, receiver operating characteristic curves, and the corresponding area under the curve (AUC). The optimal model was selected based on AUC in conjunction with balanced sensitivity and specificity.

Declarations

Author contributions statement

Q.L., C.W., and L.D. conceived and supervised the study and acquired funding. M.L. and Y.J. designed the experiments, performed the major investigations, and analyzed the data. M.L. wrote the original draft of the manuscript. Y.H., W.C., and Y.L contributed to methodology development and experimental investigation. D.L., Y.W., Q.Q., J.Z., Y.Z., S.Y., X.H., and Z.Z. carried out the patient sample collection and preparation.Y.L. and J.Y. performed machine learning related analysis and data processing. C.W., Q.L., L.D., and W.C. reviewed and edited the manuscript. All authors discussed the results and approved the final manuscript.

Competing interests

The authors declare no competing interests.

Author Contribution

Q.L., C.W., and L.D. conceived and supervised the study and acquired funding. M.L. and Y.J. designed the experiments, performed the major investigations, and analyzed the data. M.L. wrote the original draft of the manuscript. Y.H., W.C., and Y.L contributed to methodology development and experimental investigation. D.L., Y.W., Q.Q., J.Z., Y.Z., S.Y., X.H., and Z.Z. carried out the patient sample collection and preparation.Y.L. and J.Y. performed machine learning related analysis and data processing. C.W., Q.L., L.D., and W.C. reviewed and edited the manuscript. All authors discussed the results and approved the final manuscript.

Acknowledgement

This study was supported by the National Natural Science Foundation of China (NO. 32271427, 32471433, and 32071370), and Concept Validation Project of the First Affiliated Hospital of Xi'an Jiaotong University (NO. GNYZ202503).

Data Availability

All data supporting the findings of this study are available within the paper and its Supplementary Information.

References

1. Carpenter, G. & Brewer, M. R. EpCAM: Another Surface-to-Nucleus Missile. *Cancer Cell* 15, 165–166, doi:10.1016/j.ccr.2009.02.005 (2009).
2. Kong, H. *et al.* Dual-color fluorescence detection of tumor-derived extracellular vesicles using a specific and serum-stable membrane-fusion approach. *Biosens Bioelectron* 278, 117302,

doi:10.1016/j.bios.2025.117302 (2025).

3. Hsu, Y.-T. *et al.* EpCAM-Regulated Transcription Exerts Influences on Nanomechanical Properties of Endometrial Cancer Cells That Promote Epithelial-to-Mesenchymal Transition. *Cancer Res* 76, 6171–6182, doi:10.1158/0008-5472.Can-16-0752 (2016).
4. Fagotto, F. & Aslemarz, A. EpCAM cellular functions in adhesion and migration, and potential impact on invasion: A critical review. *Biochim Biophys Acta Rev Cancer* 1874, 188436, doi:10.1016/j.bbcan.2020.188436 (2020).
5. Yu, S. *et al.* A single-sEV analysis identifies plasma EPCAM+sEVs as a biomarker for early diagnosis and monitoring postoperative remission of thyroid cancer. *Extracellular vesicles and circulating nucleic acids* 6, 982–999, doi:10.20517/evcna.2025.93 (2025).
6. Menz, A. *et al.* Epithelial Cell Adhesion Molecule (EpCAM) Expression in Human Tumors: A Comparison with Pan-Cytokeratin and TROP2 in 14,832 Tumors. *Diagnostics (Basel)* 14, 1044, doi:10.3390/diagnostics14101044 (2024).
7. Moiseeva, E. *et al.* Profiling of CD63 and EpCAM Membrane Proteins of Extracellular Vesicles on Tannic Acid-Coated Magnetic Beads Using Conventional Flow Cytometry. *Int J Mol Sci* 26, 11324, doi:10.3390/ijms262311324 (2025).
8. Mukherjee, S. *et al.* 2D graphene-based advanced nanoarchitectonics for electrochemical biosensors: Applications in cancer biomarker detection. *Biosens Bioelectron* 250, 116050, doi:10.1016/j.bios.2024.116050 (2024).
9. Karim, M. M. & Lasker, T. Electrochemical Biosensors for Cancer Biomarker Detection: Basic Concept, Design Strategy and Cutting-Edge Development. *Electrochemical Science Advances* 5, e70007, doi:10.1002/elsa.70007 (2025).
10. Qin, Z. *et al.* Label-free electrochemical biosensor based on AuNPs and PCL-b-PHEAA amphiphilic copolymer for highly sensitive detection of CEA. *Microchimica Acta* 192, 207, doi:10.1007/s00604-025-07063-7 (2025).
11. Yang, J. *et al.* Electrochemical biosensor based on Novozym 435 enzymatic ring-opening polymerization for CEA detection. *J Electroanal Chem* 977, 118846, doi:10.1016/j.jelechem. 2024.118846 (2025).
12. Brahmi, M. & Bakirhan, N. K. Innovations in traumatic brain injury diagnostics: electrochemical impedance spectroscopy leading the way. *J Appl Electrochem* 55, 1–17, doi:10.1007/s10800-024-02159-z (2025).
13. Yang, M. Q., Wang, L., Lu, H. Z., Yang, Y. C. & Liu, S. Recent Advances of Functional Nanomaterials for Screen-Printed Photoelectrochemical Biosensors. *Acta Phys-chim Sin* 41, 100018, doi:10.3866/pku.Whxb202310046 (2025).
14. Nashruddin, S. N. A. B. M., Salleh, F. H. M. & Raub, A. A. M. Early detection of kidney problems through voltammetry, potentiometry, amperometry, and impedance electrochemical techniques: A comprehensive review. *Measurement* 230, 114475, doi:10.1016/j.measurement. 2024.114475 (2024).

15. Meza-Morales, W. *et al.* Functionalized screen-printed electrodes for non-invasive detection of vascular-endothelial cadherin in extracellular vesicles. *RSC Adv* 15, 12609–12621, doi:10.1039/d4ra08926j (2025).
16. John, J. F., Dhinasekaran, D. & Subashchandran, S. On-site detection of uric acid using a portable electrochemical device based on a screen-printed electrode modified with nickel ferrite. *Mater Today Chem* 47, 102787, doi:10.1016/j.mtchem.2025.102787 (2025).
17. Lakshmipriya, T. & Gopinath, S. C. B. Antibody-aptamer Complementation: Advancing Biosensing for Disease Monitoring. *Curr. Top. Med. Chem.* 26, 238–249, doi:10.2174/0115680266372074250603091350 (2026).
18. Li, M. *et al.* Highly efficient and label-free sensitive detection of tumor-derived exosome with an aptasensor-based microfluidic chip. *Microchem J* 203, 110875, doi:10.1016/j.microc. 2024.110875 (2024).
19. Mayol, B. *et al.* Aptamer and Oligonucleotide-Based Biosensors for Health Applications. *Biosensors-Basel* 15, 277, doi:10.3390/bios15050277 (2025).
20. Wang, W. J. *et al.* A Brief Review of Aptamer-Based Biosensors in Recent Years. *Biosensors-Basel* 15, 120, doi:10.3390/bios15020120 (2025).
21. Wang, Y. *et al.* Methylene Blue-Stained Single-Stranded DNA Aptamers as a Highly Efficient Electronic Switch for Quasi-Reagentless Exosomes Detection: An Old Dog with New Tricks. *Anal Chem* 95, 18166–18173, doi:10.1021/acs.analchem.3c03715 (2023).
22. Singh, R., Gupta, R., Bansal, D., Bhateria, R. & Sharma, M. A Review on Recent Trends and Future Developments in Electrochemical Sensing. *Acs Omega* 9, 7336–7356, doi:10.1021/acsomega.3c08060 (2024).
23. Masud, Song, J., Ahmed, F. & Kim, J. 2D Materials: From Design and Synthesis to Applications in Electrical and Electrochemical Biosensors. *Small* 21, e04955 doi:10.1002/smll.202504955 (2025).
24. Qin, R. *et al.* Recent Advances in Flexible Pressure Sensors Based on MXene Materials. *Adv Mater* 36, 2312761, doi:10.1002/adma.202312761 (2024).
25. Lan, L. *et al.* Two-dimensional MBenes with ordered metal vacancies for surface-enhanced Raman scattering. *Nanoscale* 15, 2779–2787, doi:10.1039/d2nr06280a (2023).
26. Yang, S. Y. *et al.* MBene Nanosheets with DNA Adsorbability for Circulating Tumor DNA Assay via Fluorescence Biosensing and Paper-Based Microfluidic POCT. *Adv Funct Mater* 35, 2415074, doi:10.1002/adfm.202415074 (2025).
27. Ma, J. L. *et al.* Efficient production of syngas and lactic acid via CrB MBene/Cd0.8Zn0.2S Schottky heterojunction photocatalysis. *Applied Catalysis B-Environment and Energy* 367, 125101, doi:10.1016/j.apcatb.2025.125101 (2025).
28. Li, Z. F. *et al.* Application of transition metal boride nanosheet as sulfur host in high loading Li-S batteries. *Chem Eng J* 452, 139366, doi:10.1016/j.cej.2022.139366 (2023).
29. Zhang, H. M., Xiang, H. M., Dai, F. Z., Zhang, Z. L. & Zhou, Y. C. First demonstration of possible two-dimensional MBene CrB derived from MAB phase Cr2A1B2. *J Mater Sci Technol* 34, 2022–2026,

doi:10.1016/j.jmst.2018.02.024 (2018).

30. Aghamohammadi, P. *et al.* CrB MBene: Synthesis, structural insights, and electrochemical performance assessment. *J Alloy Compd* 1040, 183679, doi:10.1016/j.jallcom.2025.183679 (2025).
31. Xiong, W. *et al.* Rapid synthesis of two-dimensional MoB MBene anodes for high-performance sodium-ion batteries. *J Mater Sci Technol* 212, 67–76, doi:10.1016/j.jmst.2024.05.060 (2025).
32. Quan, S. H. *et al.* CrB MBene-infused sprayable hydrogel for NIR-I/II photothermal cancer treatment. *Science China-Chemistry*, 2059–2072, doi:10.1007/s11426-025-2916-5 (2025).
33. James, A. L. & Jasuja, K. Chelation assisted exfoliation of layered borides towards synthesizing boron based nanosheets. *RSC Adv* 7, 1905–1914, doi:10.1039/c6ra26658d (2017).
34. Peak, D., Luther, G. W. & Sparks, D. L. ATR-FTIR spectroscopic studies of boric acid adsorption on hydrous ferric oxide. *Geochim Cosmochim Ac* 67, 2551–2560, doi:10.1016/s0016-7037(03)00096-6 (2003).
35. Zhang, C. C. J., Gao, X. T. & Yilmaz, B. Development of FTIR Spectroscopy Methodology for Characterization of Boron Species in FCC Catalysts. *Catalysts* 10, 1327, doi:10.3390/catal10111327 (2020).
36. Hayat, A. *et al.* Novel 2D MBenes-synthesis, structure, properties with excellent performance in energy conversion and storage: A review. *Mat Sci Eng R* 159, 100796, doi:10.1016/j.mser.2024.100796 (2024).
37. Xu, T. J. *et al.* A Rising 2D Star: Novel MBenes with Excellent Performance in Energy Conversion and Storage. *Nano Micro Lett* 15, 6, doi:10.1007/s40820-022-00976-5 (2023).
38. Yang, S. H., Zhang, F. F., Wang, Z. H. & Liang, Q. L. A graphene oxide-based label-free electrochemical aptasensor for the detection of alpha-fetoprotein. *Biosens Bioelectron* 112, 186–192, doi:10.1016/j.bios.2018.04.026 (2018).
39. Yang, S. Y. *et al.* MBene as novel and effective electrochemical material used to enhance paper-based biosensor for point-of-care testing ctDNA from mice serum. *Chem Eng J* 498, 155345, doi:10.1016/j.cej.2024.155345 (2024).
40. Noureen, B. *et al.* Light-addressable potentiometric sensors modified with mesoporous silica nanoparticles for label-free detection of adenosine. *Talanta* 297, 128759, doi:10.1016/j.talanta.2025.128759 (2026).
41. Ullah, N. *et al.* Label-Free Detection of Saxitoxin with Field-Effect Device-Based Biosensor. *Nanomaterials* 12, 1505, doi:10.3390/nano12091505 (2022).
42. Liu, Y. P. *et al.* A facile liquid biopsy assay for highly efficient CTCs capture and reagent-less monitoring of immune checkpoint PD-L1 expression on CTCs with non-small cell lung cancer patients. *Biosens Bioelectron* 275, 117236, doi:10.1016/j.bios.2025.117236 (2025).
43. Jalil, O., Pandey, C. M. & Kumar, D. Highly sensitive electrochemical detection of cancer biomarker based on anti-EpCAM conjugated molybdenum disulfide grafted reduced graphene oxide nanohybrid. *Bioelectrochemistry* 138, 107733, doi:10.1016/j.bioelechem.2020.107733 (2021).

44. Guo, X. *et al.* Tetrahedron Probes for Ultrasensitive In Situ Detection of Telomerase and Surface Glycoprotein Activity in Living Cells. *Anal Chem* 92, 2310–2315, doi:10.1021/acs.analchem.9b05180 (2020).
45. Shiddiky, M. J. A., Rauf, S., Kithva, P. H. & Trau, M. Graphene/quantum dot bionanoconjugates as signal amplifiers in stripping voltammetric detection of EpCAM biomarkers. *Biosens Bioelectron* 35, 251–257, doi:10.1016/j.bios.2012.02.057 (2012).
46. Sweety, Paneru, S. & Kumar, D. CuS modified PEDOT:PSS grafted paper-based electrochemical immunosensor for EpCAM biomarker detection. *Mater Chem Phys* 313, 128687, doi:10.1016/j.matchemphys.2023.128687 (2024).
47. Ma, Y. *et al.* Aptamer-functionalized quasi-ZIF-67@methylene blue hybrid nanoprobes for the electrochemical aptasensing of epithelial cancer biomarkers. *Chem Eng J* 483, 149362, doi:10.1016/j.cej.2024.149362 (2024).
48. Wang, P. L. *et al.* Highly selective detection of breast cancer cells mediated by multi-aptamer and dye-loaded mesoporous silica nanoparticles. *Microchimica Acta* 191, 577, doi:10.1007/s00604-024-06664-y (2024).
49. Wu, Y. J., Wang, Y., He, R. X., Li, Y. & Ben, Y. L. A dual-signal-amplified electrochemical biosensor for sensitive and accurate detection of cancer cells. *RSC Adv* 15, 32546–32552, doi:10.1039/d5ra00364d (2025).
50. Xu, J. G., Wang, X. X., Yan, C. & Chen, W. A Polyamidoamine Dendrimer-Based Electrochemical Immunosensor for Label-Free Determination of Epithelial Cell Adhesion Molecule- Expressing Cancer Cells. *Sensors* 19, 1879, doi:10.3390/s19081879 (2019).
51. Shen, H. W. *et al.* A novel label-free and reusable electrochemical cytosensor for highly sensitive detection and specific collection of CTCs. *Biosens Bioelectron* 81, 495–502, doi:10.1016/j.bios.2016.03.048 (2016).
52. Luo, J. R. *et al.* Highly sensitive photoelectrochemical sensing platform based on PM6:Y6 p-n heterojunction for detection of MCF-7 cells. *Sensor Actuat B-chem* 363, 131814, doi:10.1016/j.snb.2022.131814 (2022).
53. Li, X. T. *et al.* Simultaneous detection of MCF-7 and HepG2 cells in blood by ICP-MS with gold nanoparticles and quantum dots as elemental tags. *Biosens Bioelectron* 90, 343–348, doi:10.1016/j.bios.2016.11.030 (2017).
54. Madár, I. *et al.* Diagnostic Accuracy of Transvaginal Ultrasound and Magnetic Resonance Imaging for the Detection of Myometrial Infiltration in Endometrial Cancer: A Systematic Review and Meta-Analysis. *Cancers* 16, 907, doi:10.3390/cancers16050907 (2024).
55. Li, J., Wang, X., Qu, W., Wang, J. & Jiang, S. W. Comparison of serum human epididymis protein 4 and CA125 on endometrial cancer detection: A meta-analysis. *Clin Chim Acta* 488, 215–220, doi:10.1016/j.cca.2018.11.011 (2019).
56. Gentry-Maharaj, A. & Karpinskyj, C. Current and future approaches to screening for endometrial cancer. *Best practice & research. Clinical obstetrics & gynaecology* 65, 79–97,

doi:10.1016/j.bpobgyn.2019.12.006 (2020).

57. Han, L. *et al.* An Efficacious Endometrial Sampler for Screening Endometrial Cancer. *Front Oncol* 9, 67, doi:10.3389/fonc.2019.00067 (2019).

Figures

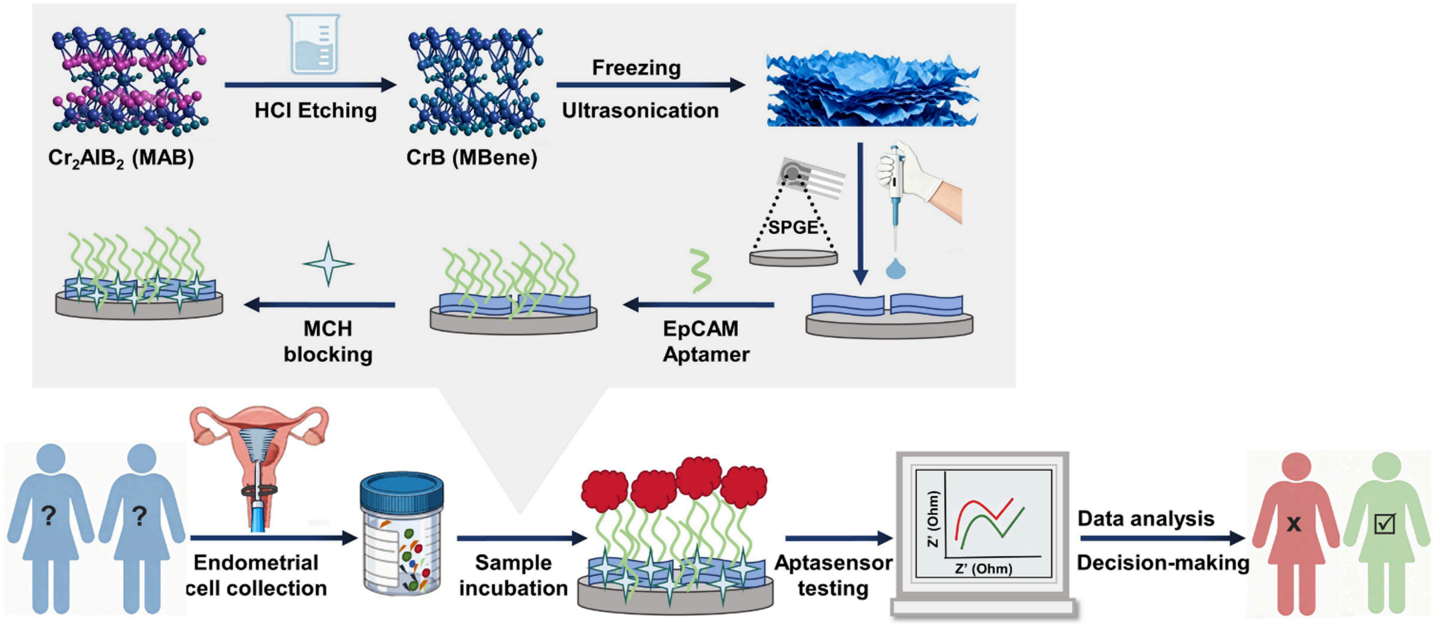


Figure 1

MBene-based electrochemical aptasensor platform for label-free detection of EpCAM-overexpressing cancer cells. Schematic illustration shows the stepwise assembly of the aptasensing interface, electrochemical detection mechanism, and preliminary validation using patient-derived clinical samples.

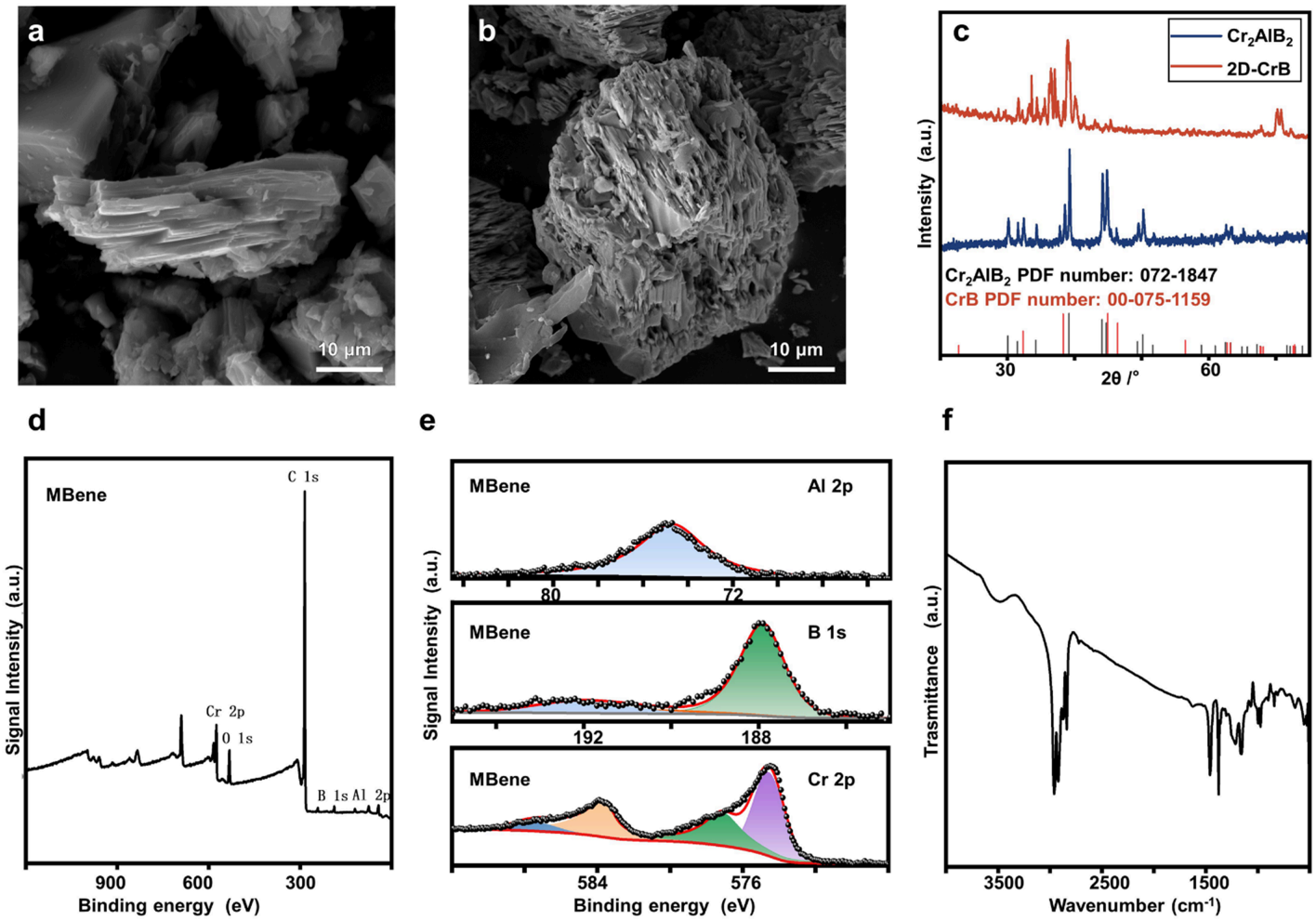


Figure 2

Characterization of MBene nanosheets. (a) SEM image of the Cr_2AlB_2 MAB precursor. **(b)** SEM image of the etched two-dimensional CrB MBene nanosheets. **(c)** XRD patterns of Cr_2AlB_2 and CrB MBene. **(d)** XPS survey spectrum of CrB MBene nanosheets. **(e)** XPS spectra of Al 2p, B 1s, and Cr 2p for CrB MBene nanosheets. **(f)** FTIR spectrum of CrB MBene nanosheets.

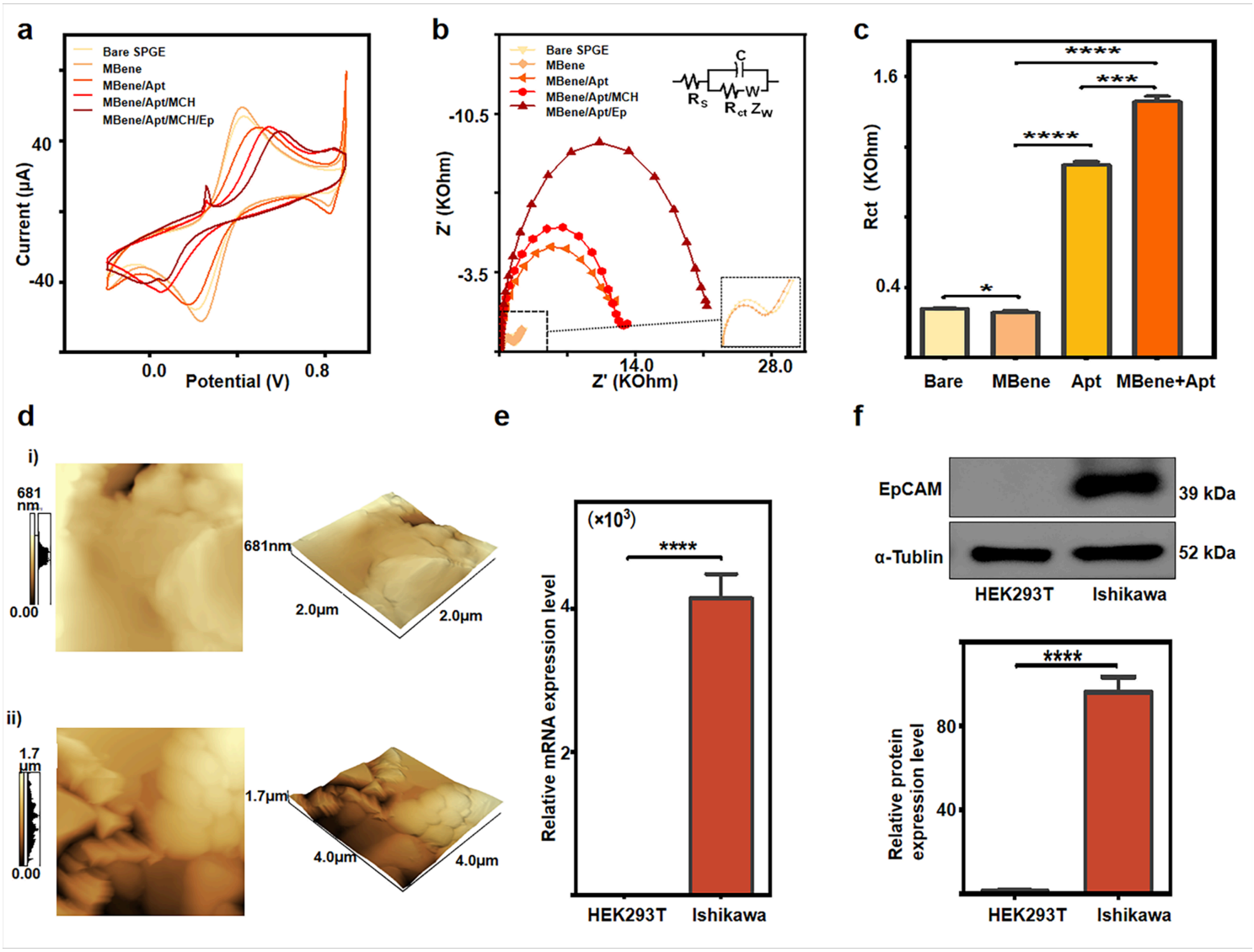


Figure 3

Characterization of the stepwise assembly of the electrochemical aptasensor and validation of EpCAM expression in cell lines. (a-c) Cyclic voltammetry (CV) curves, electrochemical impedance spectroscopy (EIS) Nyquist plots, and corresponding relative charge transfer resistance ($\triangle R_{ct}$) values of bare and modified electrodes. EIS data were fitted using the equivalent circuit model ($R_s/C/Rct/Z_w$). **(d)** AFM images of the surface topography for i) bare SPGE and ii) the final EpCAM/MCH/Aptamer/MBene/SPGE biosensor. **(e)** Relative mRNA expression levels of EpCAM in HEK293T and Ishikawa cells determined by qRT-PCR. **(f)** Western blotting analysis and corresponding quantitative analysis of EpCAM protein levels in HEK293T and Ishikawa cell lines. Error bars represent the standard deviation of three independent experiments (n = 3). *$p < 0.05$, ***$p < 0.001$, ****$p < 0.0001$.

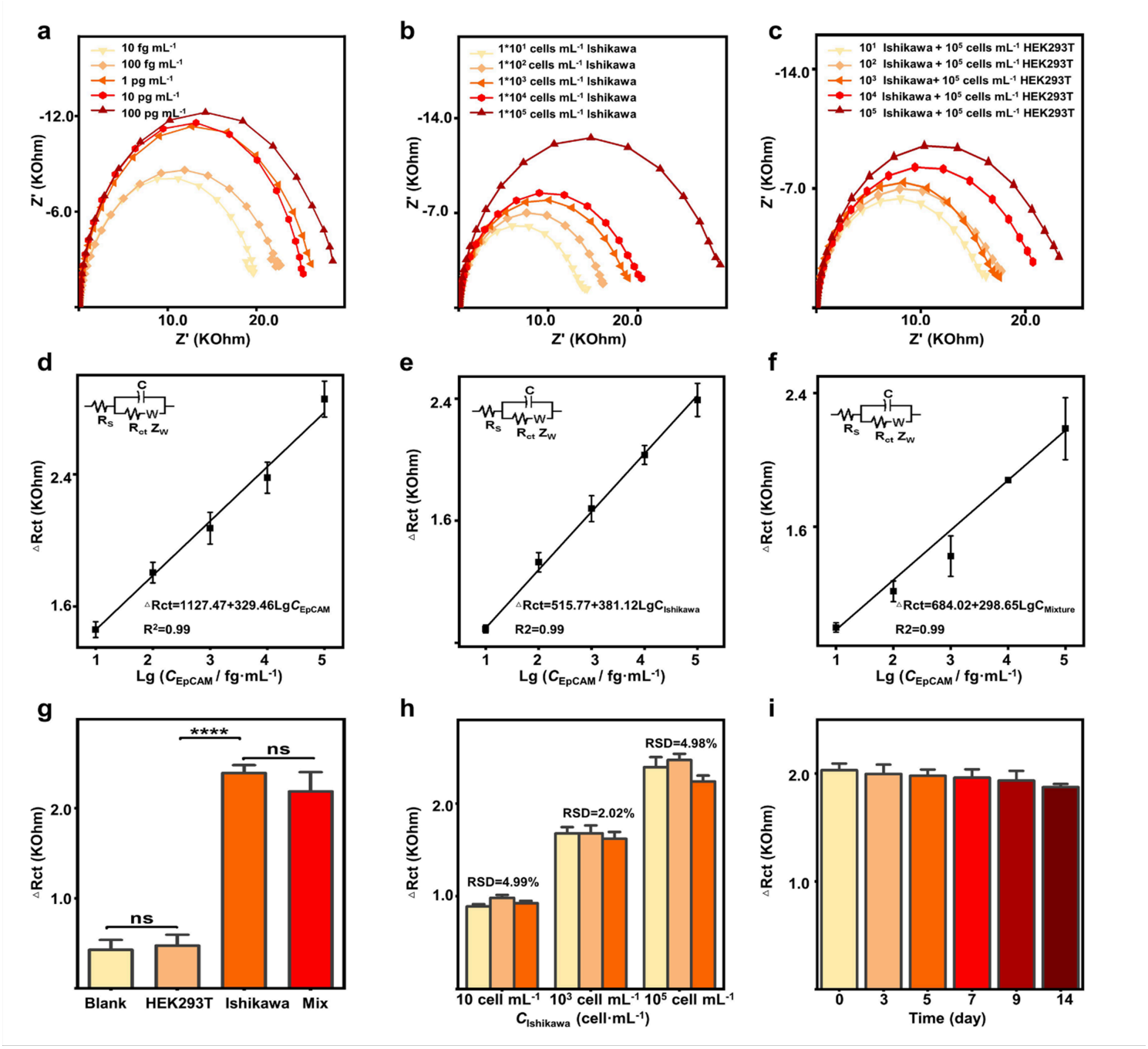


Figure 4

Electrochemical analytical performance of the MCH/Aptamer/MBene/ SPGE biosensor. (a-c) Representative Nyquist plots recorded for different concentrations of EpCAM protein, Ishikawa cells, and Ishikawa cells spiked with 10^5 cells/mL HEK293T, respectively. **(d-f)** Corresponding linear regression plots of $\triangle R_{ct}$ versus the logarithm of concentrations for EpCAM protein, Ishikawa cells, and Ishikawa cells in the presence of interfering HEK293T cells, respectively. **(g)** Specificity evaluation using PBS blank control, HEK293T cells, Ishikawa cells and mixed cell samples. The concentration of all cell sampels was 10^5 cells mL^{-1}. **(h)** Reproducibility assessment using three independently fabricated electrodes for detecting Ishikawa cells at the concentrations of 10^1, 10^3, and 10^5 cells mL^{-1}. **(i)** Storage stability of the

aptasensor evaluated over different periods at 4°C. Error bars represent the standard deviation of three independent experiments (n = 3). ****$p < 0.0001$.

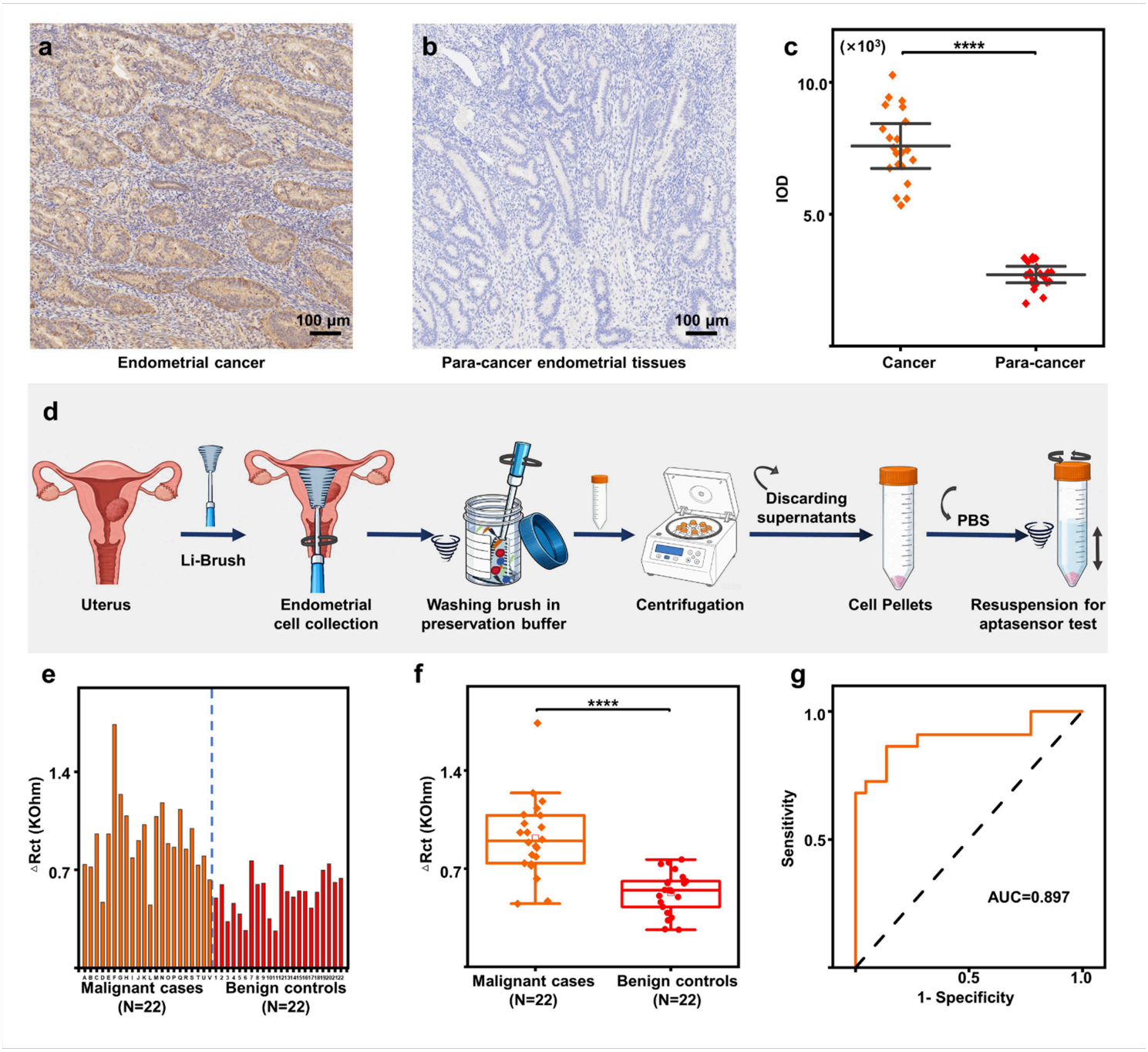


Figure 5

Clinical validation of the MCH/Aptamer/MBene/SPGE biosensor using patient-derived clinical samples. **(a-b)** Representative immunohistochemical staining images of EpCAM in malignant endometrial tissues and adjacent non-cancerous endometrial tissues. **(c)** Quantitative comparison of integrated optical density (IOD) values for EpCAM expression between malignant and adjacent non-cancerous tissues. **(d)** Schematic illustration of the collection and preparation process for clinical endometrial cytological samples via Li-Brush. **(e)** Individual EIS response ($\triangle R_{ct}$) of malignant cases (n=22) and benign controls

(n=22) from clinical endometrial cytological samples. **(f)** Boxplot comparison of electrochemical responses between malignant and benign endometrial cytological samples. **(g)** Receiver operating characteristic curve based on electrochemical response data using a logistic regression model for discrimination between malignant and benign cases. ****$p < 0.0001$.

Supplementary Files

This is a list of supplementary files associated with this preprint. Click to download.

- Supplementalmaterial.docx